

The cosmology dependence of weak lensing cluster counts

Laura Marian^{1,2}, Robert E. Smith³, Gary M. Bernstein¹

*Department of Physics and Astronomy, University of Pennsylvania, Philadelphia, PA 19104, USA*¹
*Argelander-Institut für Astronomie, Universität Bonn, Bonn, D-53121, Germany*²
Institute for Theoretical Physics, University of Zürich, Zürich, CH 8037, Switzerland^{3*}

We present the main results of a numerical study of weak lensing cluster counting. We examine the scaling with cosmology of the projected-density-peak mass function. Our main conclusion is that the projected-peak and the three-dimensional mass functions scale with cosmology in an astonishingly close way. This means that, despite being derived from a two-dimensional field, the weak lensing cluster abundance can be used to constrain cosmology in the same way as the three-dimensional mass function probed by other types of surveys.

Introduction—Weak gravitational lensing (WL) has long been recognized as a powerful cosmological probe. Among the WL observables are the peaks in shear or convergence maps, which can be used to detect clusters as points with high signal-to-noise ratio (S/N). The number of clusters per unit mass per unit volume, also known as the mass function, $dN/dV/d\log M$ is sensitive to various cosmological parameters, such as Ω_m —the matter density parameter, σ_8 —the normalization of the power spectrum, and w_0, w_a —the dark energy equation of state. Regardless of the way clusters are detected, the standard approach to constrain cosmology is to compare their distribution $dN/dV/d\log M$ to mass functions measured from N -body simulations or to the predictions of the semi-analytical theories such as [1, 2, 3, 4]. In the case of WL, this procedure has the caveat that shear peaks offer a two-dimensional statistic, while the above-mentioned mass functions represent a three-dimensional one: shear peaks can be created by large virialized clusters, but also by small undetectable clusters, and unvirialized structures projected along the line of sight. This is known as the projection effect, a major source of uncertainty in forecasts of the detection rates and cosmological power of WL cluster-counting surveys.

The fundamental assumption used in WL-cluster forecasts [5, 6] is that the shear-peak mass function is *the same* as the three-dimensional one: given a shear map, once we have a reliable method to find the peaks, we can use their distribution to derive cosmological constraints. However, since line-of-sight projections alter the shear signal of clusters, we do not know if the abundance of shear peaks depends on cosmology in the same way as the abundance of virialized clusters.

Several studies in the literature have examined the projection effect. [7, 8] has shown that cluster mass determination from WL measurements can have errors of up to 20% solely due to line-of-sight projections. See also the related work of [9]. Other numerical studies [10, 11, 12, 13] have compared shear-selected cluster catalogs to those generated by traditional three-dimensional methods such as the FoF algorithm [14]. They have found the relationship between the measured shear peaks

and the expected shear signal produced by the three-dimensional clusters of their catalogs to be biased and scattered.

In this Letter, we shall test this fundamental assumption and consider the following questions: what is the abundance of shear-selected clusters, i.e. the projected mass function? How does it vary with cosmology? These two questions mostly determine the cosmological utility of a WL cluster catalog. We shall address them numerically. Pioneering work on this topic has been done by [15, 16]. They compare several cosmological models and use the aperture mass technique of [17] to conclude that the shear-derived cluster abundance is in reasonable agreement with the Press-Schechter theory. The conclusions which we draw are based on the analysis of a large ensemble of 32 N -body simulations, sampling four different cosmological models with eight realizations per model. Our results therefore have more statistical power than previous studies, since we have a significantly larger sample volume and also a larger number of independent realizations per model. This latter fact enables us to place robust ensemble-averaged errors on our results.

In a WL map, the line-of-sight structures which contribute to a cluster's signal can be nearby the cluster, in which case they are correlated with it, or they can be at large distances adding accidentally to the signal of the cluster. Therefore, we can distinguish between *correlated* and *uncorrelated* projections. Our focus here is *only* on correlated projections: we divide our simulation volume into slabs with thickness in the range where the cluster correlation function is significant. We defer estimating the impact of chance projections to future work, as they require very large simulation volumes. In addition, previous studies have found chance projections to be of small significance, e.g. see [5, 10, 12]. From the simulations, we measure the peaks in the projected density field at a redshift of interest for weak lensing surveys, $z = 0.3$. For the same redshift, we then measure the three-dimensional mass function of the halos and compare to the projected-peak mass function and also to the theoretical prediction of [2]. The projected density field is not a WL observable. However, since we do work in

thin slabs, it is equal to the convergence up to a proportionality constant. This is a simplified case, but should the projected-peak mass function thus measured behave very differently than the prediction of [2], we expect that in a more realistic scenario, where convergence or shear peaks are measured, the discrepancy would only increase. We would also like to separate very cleanly the impact on the two-dimensional mass function of the correlated projection bias from biases induced by other WL survey systematics, such as shape noise.

Methodology—We have used Gadget2 [18] to generate simulations with 400^3 particles in a volume of 512^3 (Mpc/h) 3 ; the simulations were started at $z = 50$, and the initial conditions were generated with 2LPT [19]. For each of the eight realizations, the initial conditions for the four cosmologies are the same. This matching of initial conditions will minimize the cosmic variance on the comparison of mass functions in different cosmologies.

Given our focus on correlated projections, we divide each simulation cube into 10 slabs normal to the chosen line of sight. Each slab has a thickness of ≈ 50 Mpc/h, which is the range where the cluster correlation function is significant. We convolve the projected matter density in these slabs with an optimal filter, to find the density peaks. The filter we use is similar to that described in [5]. To every point in the filtered density field map we associate a mass given by:

$$M(\mathbf{x}_0) = \int d^2x W(\mathbf{x}_0 - \mathbf{x})\Sigma(\mathbf{x}), \quad (1)$$

where W is our filter and Σ denotes the projected density of dark matter. W is an optimal filter, i.e. it maximizes the S/N. W is tuned to best recover halos with Navarro-Frenk-White (NFW) density profiles, but with masses defined by Sheth-Tormen (ST): if a peak identified in the projected density map corresponds to such a cluster, then the filter will return the ST mass of that cluster at the position of the peak. ST virial radii, concentrations, and masses are larger than the NFW ones. We choose to normalize our filter for ST masses over NFW ones in order to get a better match with the three-dimensional halos of our simulations, which were identified with the FoF algorithm. The FoF halo mass function fits the ST mass function with an accuracy of $\approx 10\% - 20\%$. The filter satisfying these requirements is given by the expression:

$$W(\mathbf{x}) = M_{ST} \frac{\Sigma_{ST}(\mathbf{x})}{\int d\mathbf{x} |\Sigma_{ST}(\mathbf{x})|^2}, \quad (2)$$

where we have used the truncated ST projected density: $\Sigma_{ST}(x) = r_s \delta_c^{ST} \rho_m f_{ST}(x)$. r_s is the scale radius of the cluster, ρ_m is the matter density at the redshift of the halo, δ_c^{ST} is the characteristic overdensity of the profile, and f_{ST} is a function which depends on cosmology only through the concentration parameter. For its expression, see, for instance, [10].

Having filtered the two-dimensional density map, we then apply a rigorous algorithm to find the peaks. The novelty of our peak-finding algorithm is that we filter the density field recursively, with filters of decreasing mass. The highest mass peaks are identified first; smaller peaks subsequently found at the same location or within the virial radius of a higher peak are discarded. Thus the ‘‘halos in halos’’ problem is nicely solved, e.g. see [10]. Moreover, we understand the variation with cosmology of our filtered output, which is crucial for establishing the cosmology scaling of the lensing mass function. Finally, our filter has a very clear physical meaning, i.e. it returns the mass of a halo. All these features distinguish our peak-finding technique from other WL cluster studies, which use Gaussian filters of fixed size, see, for instance, [10, 11]. Full details of our projected-cluster-finding algorithm, the numerical simulations used, and an analytic model for predicting the projection noise contamination are described in a companion paper [20].

Results—In Figure 1 we present the projected-peak and the three-dimensional halo mass functions, measured from our simulations and ratioed with respect to the predictions from the ST theory. The cosmologies of the simulations assume a flat universe, with dark energy in the form of a cosmological constant. We chose our fiducial model to have $\Omega_m = 0.27$, $\sigma_8 = 0.9$. We shall refer to the other three models as the variational cosmologies, because they simply vary the matter density parameter and the amplitude of the power spectrum around the fiducial values: $\Omega_m = \{0.22, 0.32, 0.27\}$, and respectively $\sigma_8 = \{0.9, 0.9, 0.75\}$. Thus we are directly testing the cosmological dependence of the lensing mass function.

Each panel in Figure 1 corresponds to one of these models. The projected density peaks are depicted by the red solid rectangles, while the three-dimensional halos are the green empty rectangles. The error bars have been computed as errors on the mean of the eight realizations of each cosmology. For all four cosmological models, we find the mass function of three-dimensional halos comparable to that of projected peaks. The difference between the two mass functions is due to both projection effects and also to the efficiency with which we recover the halos from the projected density field. If we were to consider only the projection effects, we would expect the lensing mass function to be higher than the three-dimensional one, which it is not the case for most of the mass bins shown in Figure 1. This is mainly due to the fact that we compare peaks found with a spherical-overdensity (SO) filter to FoF halos. FoF and SO masses are known to differ, because the FoF algorithm links together small halos that are close to each other, whereas the SO halo finder considers them as separate objects. For a rigorous analysis of this issue, see [4] and references therein. [21] and [22] have thoroughly investigated the correspondence between three-dimensional and two-dimensional masses of individual clusters in the presence

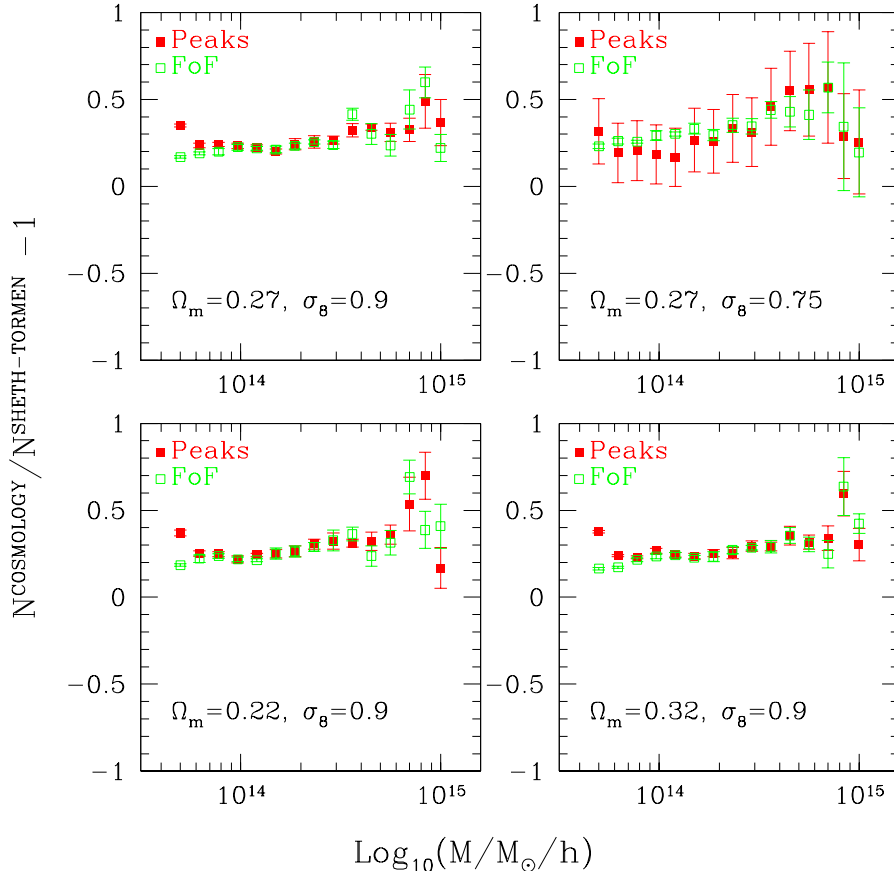


FIG. 1: The projected-peak (solid squares) and the FoF (empty squares) mass functions, scaled by the ST theory for the four cosmologies of our simulations. The error bars represent errors on the mean of the eight realizations of each cosmology.

of correlated projections and have found significant scatter between the two. The former concluded that cluster masses are overestimated due to line-of-sight projections, while the latter study attributed the scatter mostly to the triaxial nature of halos. We also found that when filtering isolated FoF halos (i.e. only the particles from a single halo), in more than 90% of cases we recover the mass to be smaller or equal to the FoF mass, which explains the trend displayed in Figure 1. It is however difficult to compare our results to these previous works, as the mean ratio of two-dimensional and three-dimensional masses depends on the mass definition and filter used. We also did not consider mass estimates averaged over several line-of-sights, as done by [21] and [22], but analyzed a much larger number of clusters.

However, our goal here is not to establish the correspondence between the two-dimensional and three-dimensional masses of individual halos, but the cosmology dependence of the shear-peak-abundance. This should be independent of the halo mass definition and

the choice of filter.

Figure 2 is the most important result of this work. It shows the mass function fractional difference of the variational models and the fiducial one, averaged over the ensemble. The fractional mass function for each model is depicted with a different symbol—circle, triangle, rectangle; the filled symbols represent projected-peaks measurements, FoF halos are the empty symbols, and finally the ST theory is shown by the starred symbols. Just like in Figure 1, the errors are on the mean of the eight realizations of the three fractional differences.

The plot shows clearly that the projection mass function varies with cosmology *in the same way* as the three-dimensional and the ST mass functions. Although this result was suggested by early studies [16], our simulations demonstrate with high statistical significance that this conclusion is robust. There are two reasons why this plot outlines unambiguously the scaling with cosmology of the lensing mass function. First, the halo finder differences that we have mentioned in the discussion of Fig-

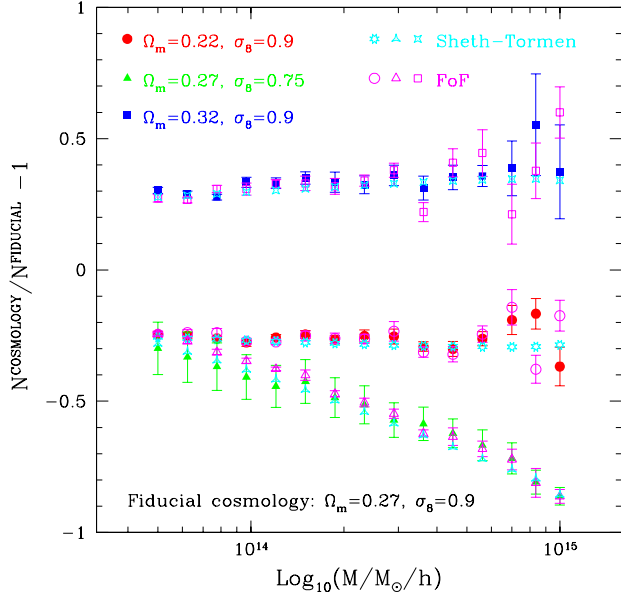


FIG. 2: The scaling with cosmology of the projected-peak mass function. The mass function for each of the three cosmologies is scaled by the fiducial cosmology mass function. The filled symbols represent projected peaks, empty symbols the FoF halos, and starred ones the ST theory. The error bars represent errors on the mean of the eight realizations of each cosmology.

ure 1 do not play a significant part here, since we take ratios of numbers of objects selected with the same type of filter. Second, we have reduced the cosmic variance of different cosmologies, due to the way we chose the initial conditions for the density fluctuations.

The most important consequence of the close cosmology scaling in Figure 2, is that we can fit the projected mass function for the fiducial model and then use the ST theory to predict the behaviour for other cosmologies. We reserve a detailed demonstration of this for our companion paper.

The results so far are very encouraging in demonstrating that the projected mass function in 50–100 Mpc slabs has very similar cosmological dependence to the better-studied virial mass functions. Some caution is necessary, however, as shear maps are linear combinations of projected density fields over many slabs along the line of sight, weighted by the lensing kernel. Additional work is needed when moving from the projected-density mass function to the shear-peak distribution function. There is great hope that the shear-peak mass function also follows the scaling with cosmology of the three-dimensional mass function. Taking this step is our goal for the near future. With the cosmological dependence of the projected mass function well understood, WL-selected cluster cata-

logs can match the statistical power of X-ray or Sunyaev-Zeldovich-selected catalogs of similar depth, but sidestep the difficult issue of calibrating the mass-observable relation.

Acknowledgements

L.M. particularly thanks Tsz Yan Lam for numerous technical discussions. We thank Ravi Sheth and Bhuvnesh Jain for access to their Opteron cluster. We are also grateful to Peter Schneider for comments on this manuscript. R.E.S. acknowledges support from a Marie Curie Reintegration Grant and the Swiss National Foundation. G.B. and L.M. were supported by NSF grant AST-0607667 and NASA grant BEFS-04-0014-0018. G.B. additionally acknowledges Department of Energy grant DOE-DE-FG02-95ER40893. L.M. is also supported by the Deutsche Forschungsgemeinschaft under the Transregion TRR33 The Dark Universe.

* Electronic address: lmarian@astro.uni-bonn.edu

- [1] W. H. Press and P. Schechter, *ApJ* **187**, 425 (1974).
- [2] R. K. Sheth and G. Tormen, *MNRAS* **308**, 119 (1999).
- [3] M. S. Warren, K. Abazajian, D. E. Holz, and L. Teodoro, *ApJ* **646**, 881 (2006).
- [4] J. Tinker, A. V. Kravtsov, A. Klypin, K. Abazajian, M. Warren, G. Yepes, S. Gottlöber, and D. E. Holz, *ApJ* **688**, 709 (2008), 0803.2706.
- [5] L. Marian and G. M. Bernstein, *Phys. Rev. D* **73**, 123525 (2006).
- [6] S. Wang, J. Khoury, Z. Haiman, and M. May, *Phys. Rev. D* **70**, 123008 (2004).
- [7] H. Hoekstra, *A&A* **370**, 743 (2001).
- [8] H. Hoekstra, *MNRAS* **339**, 1155 (2003).
- [9] S. Dodelson, *Phys. Rev. D* **70**, 023008 (2004).
- [10] T. Hamana, M. Takada, and N. Yoshida, *MNRAS* **350**, 893 (2004).
- [11] J. Y. Tang and Z. H. Fan, *ApJ* **635**, 60 (2005).
- [12] R. De Putter and M. White, *New Astronomy* **10**, 676 (2005).
- [13] J. F. Hennawi and D. N. Spergel, *ApJ* **624**, 59 (2005).
- [14] M. Davis, G. Efstathiou, C. S. Frenk, and S. D. M. White, *ApJ* **292**, 371 (1985).
- [15] G. Kruse and P. Schneider, *MNRAS* **302**, 821 (1999).
- [16] K. Reblinsky, G. Kruse, B. Jain, and P. Schneider, *A&A* **351**, 815 (1999).
- [17] P. Schneider, *MNRAS* **283**, 837 (1996).
- [18] V. Springel, *MNRAS* **364**, 1105 (2005).
- [19] M. Crocce, S. Pueblas, and R. Scoccimarro, *MNRAS* **373**, 369 (2006).
- [20] L. Marian, R. E. Smith, and G. M. Bernstein (In preparation).
- [21] C. A. Metzler, M. White, and C. Loken, *ApJ* **547**, 560 (2001), arXiv:astro-ph/0005442.
- [22] D. Clowe, G. De Lucia, and L. King, *MNRAS* **350**, 1038 (2004), arXiv:astro-ph/0402302.